On The Design of Gravity Structures using Wave Spectra

Burcharth, Hans F.; Brorsen, Michael

Publication date:
1978

Document Version
Publisher's PDF, also known as Version of record

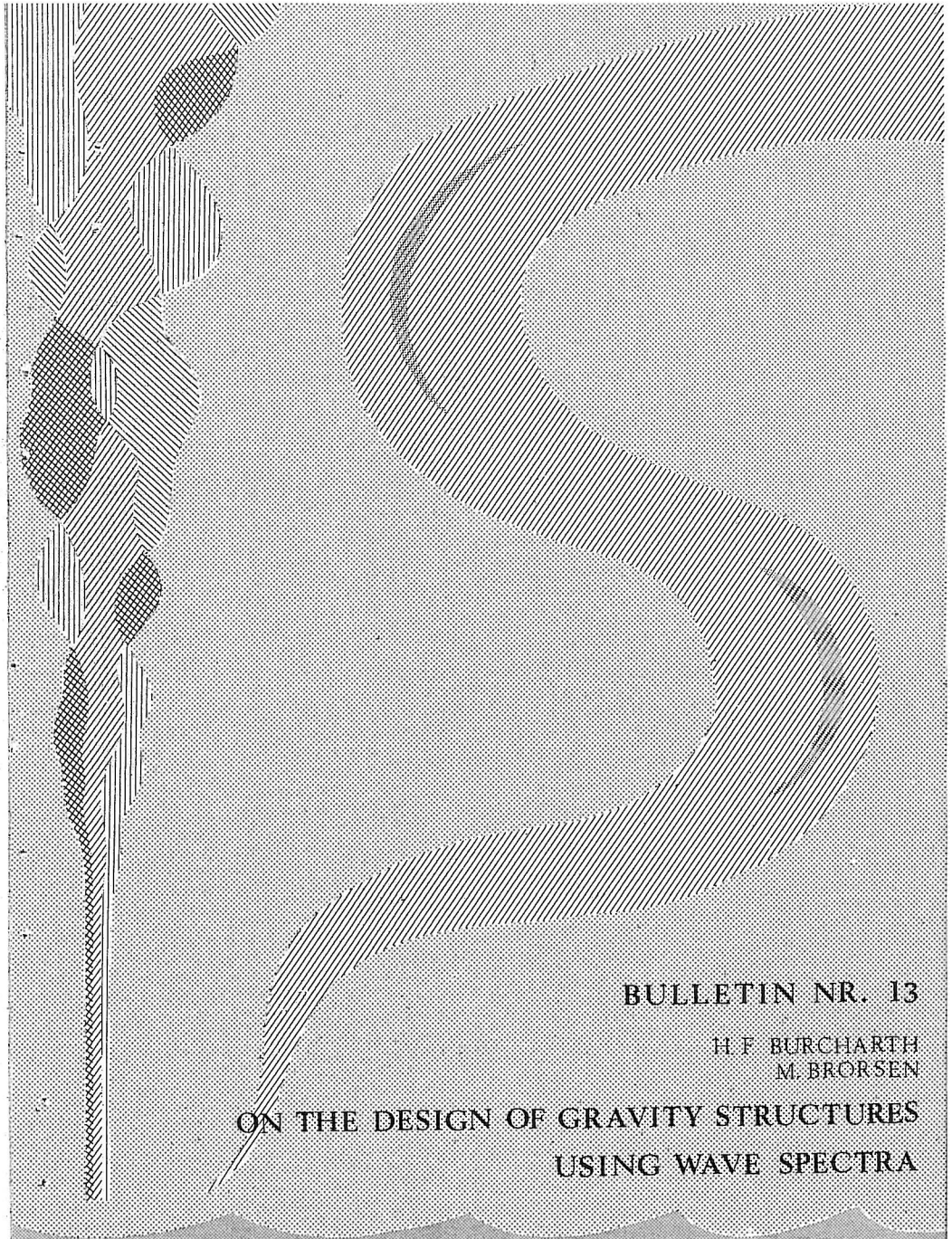

BULLETIN NR. 13

H. F. BURCHARTH
M. BRØRSEN

ON THE DESIGN OF GRAVITY STRUCTURES USING WAVE SPECTRA

AALBORG UNIVERSITETSCENTER
LABORATORIET FOR HYDRAULIK OG HAVNEBYGNING
SOHNGÅRDSHOLMSVEJ 57 DK-9000 AALBORG DANMARK

AALBORG UNIVERSITY CENTRE
INSTITUTE OF CIVIL ENGINEERING
Sohngårdsholmsvej 57 DK-9000 Aalborg Denmark Tlf. (08) 142333

HYDRAULICS LABORATORY
Bulletin no 13
May 1978

THE DESIGN OF GRAVITY STRUCTURES USING WAVE SPECTRA

H. F. Burcharth and M. Brorsen

This article represents the contents of a lecture given at Aalborg University Centre in the spring 1978. The lecture was a part of eight weekly seminars dealing with offshore engineering problems.

ON THE DESIGN OF GRAVITY STRUCTURES USING WAVE SPECTRA

H. F. BURCHARTH
professor
M. BRORSEN
ass. professor
Aalborg University Centre
Institute of Civil Engineering

CONTENTS

1. INTRODUCTION

Although most structures are subjected to dynamic, stochastic loads, it is in fact seldom that these loads are considered in the design. Normally the design is based on an equivalent static load, established naturally with due consideration to the true conditions. This method is often called deterministic, the loading being described as a specified function of time.

The deterministic method is however, inadequate for many off shore structures. In the case of gravity platforms for example this is mainly because the wave effects are the essential forces on the main frame, and these are of a stochastic nature, since they vary in time without repetition. There is therefore the possibility that the natural frequency of the structure or some part thereof, may lie in a wave frequency range with not inconsiderable energy. Resonance and the resulting amplification of forces and deformation can thus set in. There is nothing to hinder smaller waves than those chosen for a deterministic design, from causing the greatest effect. Another relevant condition, a check for fatigue, is not possible either with a deterministic method since a fatigue analysis requires precise knowledge of the cycling of the load. Such information is furthermore necessary for a more accurate determination of the wave forces, the deformation and load bearing capacity of the sea bottom, since these quantities are influenced by the response of the structure to the loading.

The purpose of this lecture is to describe a design method which takes into consideration the stochastic nature of the loading and the structures' dynamic sensitivity. The method, which can aptly be called a stochastic, dynamic response analysis, is based on the »random vibration analysis» which describes the relation between input and output of a linear, unvariant system, the input of which is given as a stationary, stochastic process. This theory was developed about 20 years ago in connection with flight problems.

We shall confine ourselves to considering the gravity platform shown in fig. 1, consisting of a bottom tank, placed directly on the sea bed, supporting a working platform by means of one or several legs.

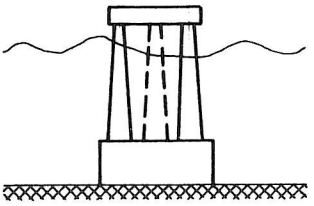

Fig. 1. Gravity platform

Since we shall only deal with wave forces for the sake of simplicity, our system consists briefly of the following:

a) Input in the form of a stochastic description of the waves.

b) Hydrodynamic transfer (or response) function which gives the relation between the waves and the wave loading on the structure.

c) Mechanical transfer function, which gives the dynamic amplification of the wave loading and thereby the final forces.

Only items a and b, i.e. the hydraulic part of the method alone, is discussed in this lecture. The lecture is furthermore concentrated on the statistic description of waves, which seems advisable as one must above all ensure reasonable input data.

Since random vibration analysis is based upon linearity we are limited right from the start to use linear wave theory as well as limit ourselves to linear wave loads. It is therefore necessary to reassure ourselves initially that these limitations are acceptable.

It should also be mentioned that, since most of the audience can only be expected to have a limited knowledge of the subject, and time is extremely short, there will be given an overall review of the subject, illustrated with some experimental results partly from the Hydraulics and Coastal Engineering Laboratory at the Aalborg University Centre, and partly from laboratories abroad.

2. GENERAL BACKGROUND

2.1 Loads due to waves

As we are discussing gravity platforms in deep water (100 - 200 m), such as in the North Sea for example, we know that higher order wave theory gives the most realistic description of storm waves. For example, up to Stokes' fifth order wave theory is used in deterministic design of structures in deep water. If we calculate wave loads in accordance with higher order stokes waves, we find that the differences in the results are rather small, the biggest jump being when we compare the linear (1. order or Airy) theory with Stokes' second order theory. Practice however showes that linear theory gives quite workable results, which, considering the uncertainty with which waves and the deformation of the subgrade, for example, are determined, leads us to the conclusion that the use of linear wave theory is an acceptable approximation.

The wave forces on a structure of the type shown in fig. 1 can be divided into 3 classes:

1. Inertia (or pressure) forces, due to acceleration of the surrounding water.
2. Drag forces, consisting of a friction and a form force due to the presence of a relative velocity between the structure and the surrounding water.
3. Shock pressure, which only accur in the surface zone with waves breaking against the structure.

We shall neglect shock loads, which have no influence on the stability or deflection of the structure, but which naturally may have a large local influence on the stresses and deformations. Shock pressure is, incidentally, a typical non-linear phenomenon, which cannot be described by Airy theory.

If we compare inertia and drag forces we find that drag forces are negible when the Keulegan - Carpenter number $N_K \leq 5$, because the diameter of both the base tank (50 - 100 m) and the legs (10 - 20 m) are not small relative to the horizontal length of the particle path. We may therefore neglect the drag forces, which is fortunate, since the principle of superposition does not hold for these forces which as we know are proportional to the square of water velocity.

We are therefore left only with inertia forces which generally can be calculated as a Froude - Krylov force multiplied by a coefficient which covers the condition that the presence of the structure modifies the undisturbed wave motion and thereby the pressure distribution. When the ratio of structure diameter to wave length $D/L \leq 0.2$ (normally the case for the legs in a storm) the inertia force, per unit length, is expressed as $\rho \frac{\pi}{4} D^2 C_M \dot{U}$, where ρ is the density of the water, C_M is a factor of about 2 and $\dot{U}$ is the horizontal acceleration of the particle. When $D/L > 0.2$ (normally always the case of a large base tank) inertia forces must be determined by means of the theory of diffraction or of the fluid finite element technique.

We must now investigate whether the principles of superposition applies to inertia forces.

Since linear wave theory has been adopted, the wave surface can be considered built up of the sum of Airy waves, the ith being defined as

$$\eta_i = a_i \sin(\omega_i t - k_i x + \delta) \tag{1}$$

where a_i is the amplitude, $\omega = 2\pi f$ is the angular frequency, t is time, $k = 2\pi/L$ is the wave number, δ is the phase angel, see fig. 2.

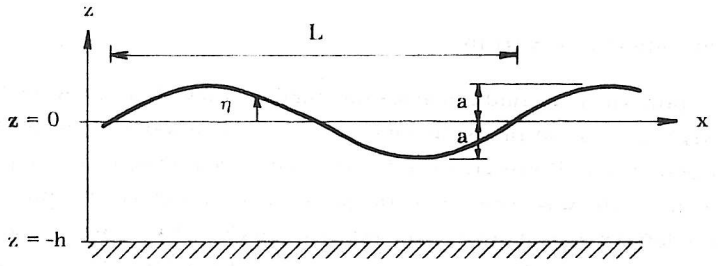

Fig. 2. Definition sketch

The deviation from hydrostatic pressure caused by waves at a point (x, z) in the ith wave is given by

$$p_i = a_i \gamma \frac{\cosh k_i(z + h)}{\cosh k_i h} \sin(\omega_i t - k_i x) \tag{2}$$

and the Froude - Krylov force on a small area dA about the point then becomes, $F_i = p_i dA$, in other words, the force amplitude is proportional to the wave amplitude.

Since the wave motion can be described as a potential flow, where the velocity potential is the sum of the potentials of the individual wave components, $\varphi = \sum_i \varphi_i$, the Froude - Krylov force from alle the wave components is found by insertion into the linearised Bernoulli's equation,

$$F = pdA = -\rho \frac{\partial \varphi}{\partial t} dA = -\rho dA \frac{\partial}{\partial t} \sum_i \varphi_i = dA \sum_i -\rho \frac{\partial \varphi_i}{\partial t} = dA \sum_i p_i \tag{3}$$

whereby it can be seen that the principle of superposition holds for forces caused by overpressures. The same applies to other quantities which are linear dependent of the velocity potential, including particle velocity and particle acceleration.

The horizontal particle velocities and accelerations for the i.th wave component at the point (x, z) is given by:

$$U_x = a_i \frac{gk_i}{\omega_i} \frac{\cosh k_i (z + h)}{\cosh k_i h} \sin(\omega_i t - k_i x) \tag{4}$$

$$\dot{U}_x = a_i g k_i \frac{\cosh k_i(z + h)}{\cosh k_i h} \cos(\omega_i t - k_i x) \tag{5}$$

i.e. proportional to wave amplitude.

2.1 Wave energy spectrum

Our first problem is to find a manageable mathematical description of the waves, apparently impossible at first sight, since wind generated waves are irregular and vary without periodicity. However, since the relevant wave forces, as seen in par. 2.1 are proportional to the wave amplitude, the position af the surface, described by a time and place defined variable vertical coordinate can give a basis for the analysis. If we measure the variation of the surface level at a fixed point we obtain a wave recording (amplitude signal) as indicated in fig. 3.

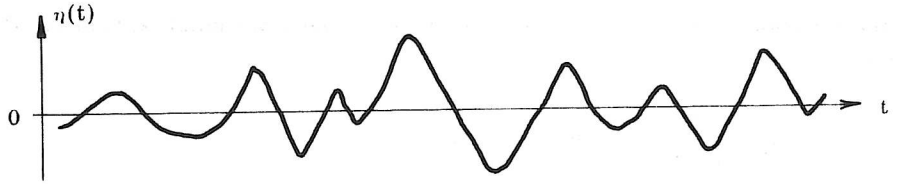

Fig. 3. Wave amplitude signal

Due to the irregular nature of the signal we naturally look for a probabilistic description of the waves. Instead of a recording such as in fig. 3 one could imagine that the water surface level was measured at a given instant in terms of a function of the horizontal coordinate in the wave direction. Such a wave recording is, however, difficult and expensive, and as one reckons that the statistic characteristics are similar for both types of signals, it is usual to use recordings at a fixed point.

With regard to the wave surface, we shall assume that it is an ergodic, stationary, Gauss-distributed, random process. An ergodic process is a process whereby the characteristics of the process can be derived by time-averaging on a single sample function instead of computing ensemble averages at specific instants of time. When dealing with wind generated waves, ergodicity is an essential prerequisite, as a single sample function in the form of a wave recording as in fig. 3 is usually the only data available. A necessary but insufficient condition for the process to be ergodic is that the process is stationary. With a single sample function we can only ensure that it is stationary. It can, however, be shown that it is reasonable to assure the process to be ergodic, if the sample function is stationary. This prerequisite of stationarity demands a sharp limitation of the length of recording, as at any given location there are usually quick variations in the wind and wave conditions. This gives in turn other problems referred to later.

Concerning the assumption that the surface elevation is Gauss (normally) distributed, it can be shown that this will be so if linear wave theory is assumed valid

and the phase shift of the components are taken evenly distributed. Wave recording analyses show furthermore that the true conditions are in fair agreement with the assumption.

Although natural waves are three-dimensional, in the following discussion we assume the waves to be long-crested. There is a short reference to experiments with three-dimensional short-crested waves later.

It is known from linear theory that the energy of a sinusoidal wave of amplitude a is $\frac{1}{2}\rho g a^2$ per unit horizontal area, where ρ is the density of the water and g is the acceleration of gravity. If linear theory and the consequent principle of superposition are valid, the wave energy can be considered made up from the energy of a series of harmonic waves each with its own frequency. By means of a harmonic analysis (Fourier or spectral analysis) of the amplitude signal we can distribute the energy to the frequencies of the various harmonic components, whereby we obtain a discrete energy spectrum as shown in fig. 4.

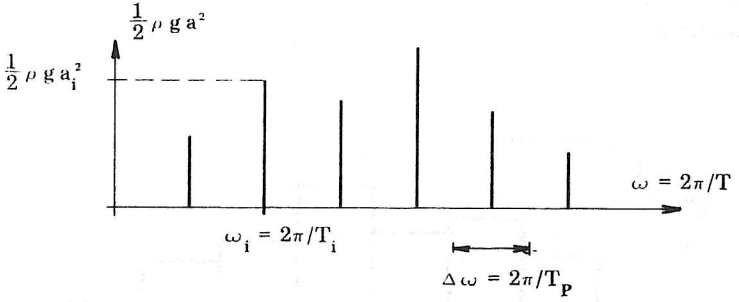

Fig. 4. Discrete wave energy spectrum

One must keep in mind that Fourier analysis really gives both a sine and cosine component for each frequency but it is usual to combine the two by inserting a phase angle δ.

$$b_i\cos(\omega_i t - k_i x) + c_i\sin(\omega_i t - k_i x) = a_i\cos(\omega_i t - k_i x - \delta_i) \tag{6}$$

where $a_i = \sqrt{b_i^2 + c_i^2}$ and $\delta_i = \tan^{-1}\frac{c_i}{b_i}$

It is thus a_i that is used in wave energy spectra, whereas δ_i is hardly ever used. One loses thereby the information that is necessary to rebuild the original wave pattern, but one can well obtain the correct wave height distribution.

Fourier analysis deals with our wave signal as a periodic signal with period T_p, which is the length of the signal. The frequency increment of the discrete spectrum will furthermore be $\Delta\omega = 2\pi/T_p$.

For simplicity we omit in the following the factor ρg in the spectrum coordinates, so that these state $\frac{1}{2}a_i^2$. In this plotting, the spectrum is called a variance spectrum, since the variance of a single cosine wave of amplitude a_i is $\frac{1}{2}a_i^2$. The variance spectrum thus shows the distribution of the signal's total variance over a series of frequencies, which are determined by the length of the signal, T_p.

As T_p approaches infinity $\Delta\omega$ approaches zero and we approach thereby a continuous spectrum, as may be seen more easily by following the stepped spectrum curve shown in fig. 5. The variance $\frac{1}{2}a_i^2$, corresponding to frequency ω_i, is assumed evenly distributed over a frequency interval $\Delta\omega$ and plotted as the area under the curve.

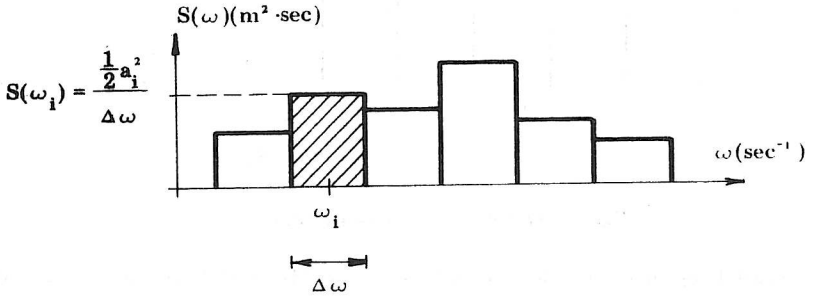

Fig. 5. Stepped variance spectrum

When $\Delta\omega$ approaches zero, the stepped curve becomes a smooth continuous curve called the continuous variance spectrum.

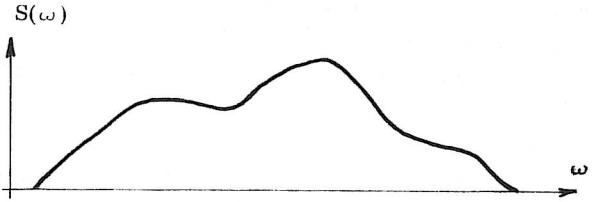

Fig. 6. Continuous variance spectrum

The area under the curve is the wave signal variance as it was for the stepped curve. In the following we refer to the continuous variance spectrum simply as the wave spectrum.

To define the form of the spectrum and it's location on the ω-axis, socalled moments are used, where the nth order moment is defined as

$$m_n = \int_0^\infty \omega^n S(\omega) d\omega \tag{7}$$

It can be seen that the zero order moment, m_0, is equal to the area under the curve, which is again equal to the signal's variance. The higher the order of the moment which is applied, the more we load the higher frequency portion of the spectrum. A broad spectrum, other things being equal, will therefore give large values of the higher order moments (for $n \geq 2$) which enables the width of the spectrum to be defined by the moments. M. S. Longuet - Higgins has thus defined a spectrum width parameter as

$$\epsilon = \sqrt{1 - \frac{m_2^2}{m_0 m_4}} \tag{8}$$

It is obvious that ϵ will have values close to zero for very narrow spectra and values close to 1 for very wide spectra. The parameter ϵ is most important on the probability distribution of waves, as we shall subsequently see.

2.3 Probability distribution of wave heights

Although the wave spectrum contains much information on the wave signal, it says nothing about how high the waves are, nor how frequently they occur, and without such information we cannot obtain a practicable description of the wave loads.

However it can be shown, as done by D. E. Cartwright and M. J. Longuet - Higgins [1], that provided the wave surface, plotted by the parameter η, fig. 3, can be taken as a stationary Grauss-distributed, random process, and provided that the wave surface can be defined by an infinite sum of cosine or sine oscillations, whose phase angles are rectangular distributed, then the frequency function (probability density) of maximum values x of the surface elevation $\eta(t)$ can be determined by

$$f(\xi) = \frac{1}{\sqrt{2\pi}} \left[\epsilon \, e^{-\frac{1}{2}\xi^2/\epsilon^2} + \sqrt{1-\epsilon^2}\, \xi \, e^{-\frac{1}{2}\xi^2} \int_{-\infty}^{\sqrt{\xi(1-\epsilon^2)}/\epsilon} e^{-\frac{1}{2}x^2} \, dx \right] \tag{9}$$

where $\xi = \frac{x}{\sqrt{m_0}}$ is a dimensionless maximum value.

For a very narrow spectrum ($\epsilon \cong 0$), (9) becomes

$$f(\xi) = \xi e^{-\frac{1}{2}\xi^2} \tag{10}$$

which is the Rayleigh distribution.

For a very wide spectrum ($\epsilon \cong 1$), (9) becomes

$$f(\xi) = \frac{1}{\sqrt{2\pi}} e^{-\frac{1}{2}\xi^2} \tag{11}$$

which is obviously the normal distribution.

The width parameter ϵ will in most storm wave spectra lie in the range 0,4-0,5. Inserting these values in (9) we find that Rayleigh distribution is a good approximation and furthermore conservative, as we obtain slightly larger waves for any given probability level.

Inserting x instead of ξ in (10) and assuming that the probability level is independent of the variable which is adopted, we obtain

$$f(\xi)d\xi = f(x)dx$$

$$f(x) = \frac{x}{m_0} e^{-\frac{x^2}{2m_0}} \tag{12}$$

Similarly the wave height H = 2x (as linear wave theory is assumed to be valid) is inserted, obtaining

$$f(H) = \frac{H}{4m_0} e^{-\frac{H^2}{8m_0}} \tag{13}$$

The corresponding distribution function for wave heights becomes

$$F(H') = P\{H < H'\} = \int_0^{H'} f(H)dH = 1 - e^{\frac{-H'^2}{8m_0}} \tag{14}$$

As can be seen from (13) and (14) with information on the wave signal's variance, m_0, alone, one can obtain the average wave height for any upper fractile of the wave recording. Referring to the deviations in [2] only the formula for average wave height $\overline{H}$ and significant wave height H_S are stated

$$\overline{H} = \sqrt{2\pi}\sqrt{m_0}$$

$$H_S = 4\sqrt{m_0} \tag{15}$$

Note that the probability distribution of the waves is fully determined by the wave spectrum, ref. (9), and thus the spectrum alone is sufficient to describe the statistics of the wave signal.

2.4 Hydrodynamic transfer function

Having dealt with the statistics of wave heights we now turn towards the relation between waves and platform loads.

Let us consider a system where an input consisting of a wave amplitude signal $\eta(t)$ defined by the spectrum $S(\omega)$ results in an output or respons $\lambda(t)$, which is the wave force signal, the characteristics of which we require, fig. 7.

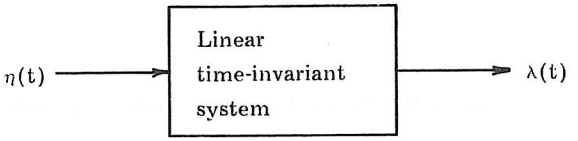

Fig. 7.

Since we are dealing with forces, as already discussed, which essentially satisfy the principle of superposition and since we can furthermore reckon that the platform dimensions will remain unchanged in time, as a close approximation we can assume that the system is linear and time-invariant.

Such a system is frequency preserving, see [3] for example. An input in the form of an oscillation of frequency ω_i, $\eta(t) = \cos\omega_i t$, will therefore give an output $\lambda(t) = |H(\omega_i)|(\cos\omega_i t - \delta_i)$, where $H(\omega_i)$, that states the relation between input and response at the given frequency, $|H(\omega_i)| = \lambda(t)/\eta(t)$, is called the frequency response function. $|H(\omega_i)|$ can be stated as the ratio of output to input amplitudes

$$|H(\omega_i)| = \frac{a_\lambda(\omega_i)}{a_\eta(\omega_i)}$$

and $|H(\omega_i)|^2$ is determined from the ratio of the variances,

$$|H(\omega_i)|^2 = \frac{\frac{1}{2}a_\lambda{}^2(\omega_i)}{\frac{1}{2}a_\eta{}^2(\omega_i)} = \frac{\sigma_\lambda{}^2(\omega_i)}{\sigma_\eta{}^2(\omega_i)}$$

We can consider the system now excited by the wave amplitude signal $\eta(t)$ defined by the spectrum $S(\omega)$. We assume furthermore that $\eta(t)$ is a stationary random process, a condition that we shall revert to subsequently.

In continuation of our earlier considerations, we now imagine $\eta(t)$ as a superposition of many independent processes, each of an infinitesimal band width, $\Delta\omega$.

For any one of these processes, centred about the frequency ω_i, the variance is

$$\sigma_\eta^2(\omega_i) = \int_{\omega_i - \Delta\omega/2}^{\omega_i + \Delta\omega/2} S(\omega)\,d\omega \cong S(\omega_i)\,\Delta\omega$$

Since $\Delta\omega$ is infinitesimal, we must expect the ratio between output and input variances will be the same as for an individual cosine, i.e.,

$$\sigma_\eta^2(\omega_i) \cong S_\eta(\omega_i)\Delta\omega \cong \frac{\sigma_\lambda^2(\omega_i)}{|H(\omega_i)|^2} \cong \frac{S_\lambda(\omega_i)\,\Delta\omega}{|H(\omega_i)|^2} \tag{16}$$

where $S_\lambda(\omega_i)$ is the value of the response spectrum at frequency ω_i. In the limit, when $\Delta\omega \to 0$, we can expect that (16) can be written as

$$|H(\omega)|^2 = \frac{S_\lambda(\omega)}{S_\eta(\omega)} \tag{17}$$

which states the relation between the input and response spectra. A rigorous mathematical derivation of this important formula can be found in [3] or [4]. The parameter $|H(\omega)|^2$ is called the transfer function. Note that the transfer function does not contain any information on the phase relations.

It is also valid for stationary random processes that are transformed by a linear time-invariant system, that the response $\lambda(t)$ will be Gauss-distributed, if such is the input, see for example [5]. Among other things, this means that the maximum values of the wave force signal, $\lambda(t)$, will have the same distribution as the wave heights of the wave amplitude signal, $\eta(t)$, which according to chapter 2.3 means a Rayleigh-distribution (provided that the wave force spectrum is a narrow spectrum).

We shall see later how the transfer function is determined, but first shall we describe how the wave energy spectrum is obtained in practice.

3. DETERMINATION OF THE WAVE ENERGY SPECTRUM

An estimate of the wave energy spectrum can be obtained by two methods different in principles.

If one or more representative wave recordings $\eta(t)$ are available an estimate of the spectrum can be obtained directly by analysing $\eta(t)$, for example by the correlation method based on the fact that the variance spectrum is the Fourier transform of the autocorrelation function, or else by the periodogram method, whereby the spectrum is obtained by means of the Fast Fourier Transform procedure (FFT) applied directly to the wave signal $\eta(t)$.

If wave recordings are not available, the energy spectrum must be estimated from the so-called standard wave energy spectra.

3.1 Corellogram method

A brief review of the method follows; for a fuller treatment see ref. [3].

The autocorrelation function, $R(\tau)$, describes the relation between the values of the function at a time, t, and it's values at another time, $t + \tau$, and it is defined as follows

$$R(\tau) = \lim_{T \to \infty} \frac{1}{T} \int_0^T \eta(t)\eta(t + \tau)\, dt \tag{18}$$

i.e. each individual plot of the correlation function is found as the product of the displaced walues of the wave signal, averaged over a period T, with $T \to \infty$. Fig. 8 gives an example of an autocorrelation function.

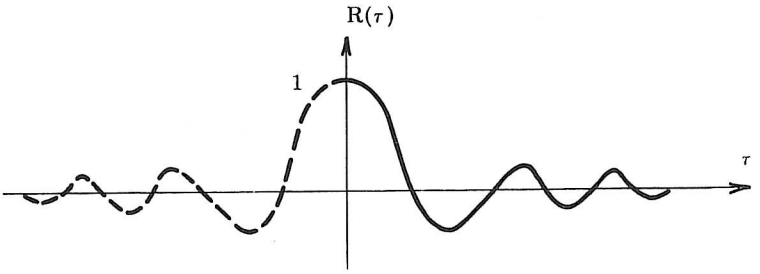

Fig. 8. Autocorrelation function

The wave energy spectrum can now be determined from the Fourier transform G(f) til $R(\tau)$, see ref. [3], i.e.

$$G(f) = \int_{-\infty}^{\infty} R(\tau) e^{-i 2\pi f \tau} \, d\tau \tag{19}$$

provided that $R(\tau)$ is absolutely integrable, $\int_{-\infty}^{\infty} |R(\tau)| d\tau < \infty$, and that $\eta(t)$ is stationary. From this expression it can be seen that G(f) is the coefficients in a Fourier series, $R(\tau)$. The requirement of stationarity, implies that $R(\tau)$ is an even function, $R(\tau) = R(-\tau)$, for which reason G(f), that must also be an even function, can be expressed as

$$G(f) = \int_{-\infty}^{\infty} R(\tau)\cos(2\pi f \tau) \, d\tau = 2 \int_{0}^{\infty} R(\tau)\cos(2\pi f \tau) \, d\tau \tag{20}$$

A Characteristic example of G(f), which because of it's symmetry about f = 0 is called the two-sided variance spectrum or the two-sided spectral density function, is shown in fig. 9.

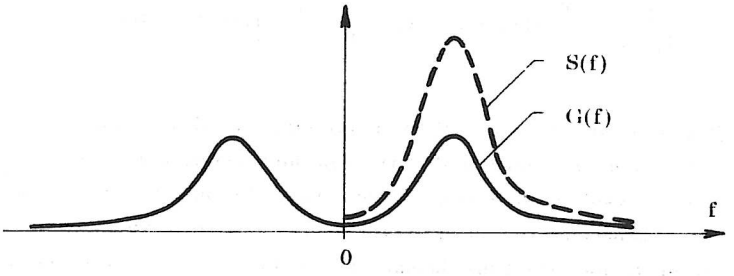

Fig. 9. One-sided and two-sided variance spectrums

Since we are dealing with frequencies ≥ 0 in real waves, the wave energy spectrum S(f) is defined as the one-sided variance spectrum in the interval $0 \leq f \leq \infty$, for which the following relation is valid, see fig. 9.

$$S(f) = 2G(f) = 2\int_{-\infty}^{\infty} R(\tau)\cos(2\pi f\tau)d\tau = 4\int_{0}^{\infty} R(\tau)\cos(2\pi f\tau)d\tau \qquad (21)$$

Since $\int_0^\infty S(f)df = \int_0^\infty S(\omega)d\omega$, (21) can be written as

$$S(\omega) = \frac{S(f)}{2\pi} = \frac{2}{\pi}\int_{0}^{\infty} R(\tau)\cos(\omega\tau)d\tau$$

When the wave signal $\eta(t)$ has to be stationary the problem will often arise, when $R(\tau)$ is to be determined in practice, that the wave records that can be used will almost always be of a very limited duration, among other reasons because the wind in any given location rarely remains constant for long. A period T_p of about 20 minutes is characteristic for storm waves signals and if we assume an average wave period of 10 seconds (North Sea) the signal will only contain 120 waves.

We cannot therefore find $R(\tau)$ from (18), since $T = T_p$ is of a limited duration, but an estimate, where we shall indeed introduce a bias error, can be obtained from

$$\hat{R}(\tau) = \frac{1}{T_p - \tau}\int_{0}^{T_p-\tau} \eta(t)\eta(t+\tau)dt \cong \frac{1}{T_p}\int_{0}^{T_p-\tau} \eta(t)\eta(t+\tau)dt \qquad (22)$$

which will give reasonable values if the maximum time displacement, τ_m, is small relative to T_p. It is also obvious that the first and second expression in (22) give unbiased and a biased estimate respectively. When the biased estimate nevertheless is often used, it is because the mean square error is smaller in this estimate.

We note now, that the time displacement from now on is only defined in the interval $0 \leq \tau \leq \tau_m$, and therefore we cannot directly determine the spectrum from the expressions (19) - (21), but must try an estimate,

$$\hat{S}(f) = 2\int_{-\tau_m}^{\tau_m} \hat{R}(\tau)\cos 2\pi f\tau\, d\tau = 2\int_{-\infty}^{\infty} u_{\tau_m}(\tau)\hat{R}(\tau)\cos 2\pi f\tau\, d\tau \qquad (23)$$

in which $u_{\tau_m}(\tau)$ is a boxcar function, which takes values 1 in the interval $-\tau_m \leq \tau \leq \tau_m$ and is otherwise zero. It is also obvious, that an estimate of the energy spectrum can be found by the Fourier transform of the function $u_{\tau_m}(\tau)\hat{R}(\tau)$.

Let us for a moment look at the influence of $u_{\tau_m}(\tau)$ by comparing the Fourier transform of $2u_{\tau_m}(\tau)R(\tau)$ with the Fourier transform of $2R(\tau)$, where the latter according to (21) is S(f).

By means of the convolution theorem we obtain

$$\hat{S}(f) = 2\int_{-\infty}^{\infty} u_{\tau_m}(\tau)R(\tau)e^{-i2\pi f\tau}d\tau = 2\int_{-\infty}^{\infty} U(\alpha)G(f-\alpha)d\alpha$$

$$\cong \int_{0}^{\infty} U(\alpha)S(f-\alpha)d\alpha \qquad (24)$$

where $U(f) = 2\tau_m \dfrac{\sin 2\pi\tau_m f}{2\pi\tau_m f}$ is the Fourier transform of $u_{\tau_m}(\tau)$, and the approximation sign in the last term is due to the fact that S(f) is not always zero near f = 0.

As the introduction of $u_{\tau_m}(\tau)$ thus results in a weighting of the spectral values with the function U(f), this function and other functions of a similar use, are

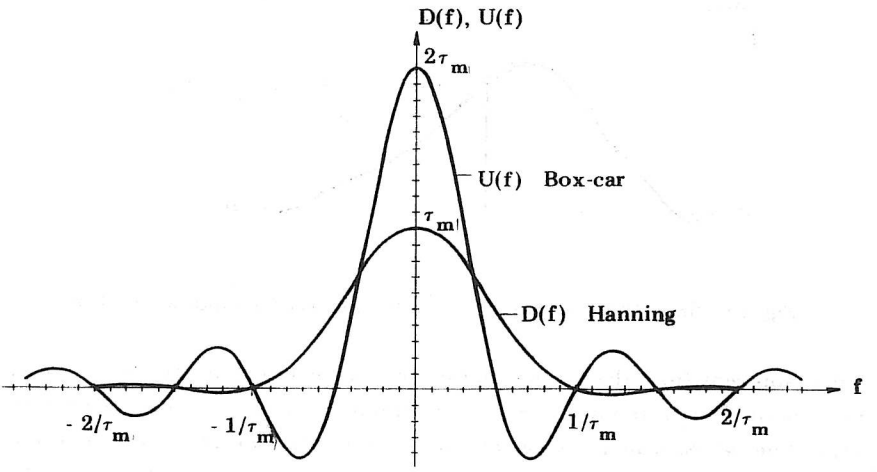

Fig. 10. Window functions in frequency domain

called weighting or window functions. Since the area under the curve U(f) = 1, the application of the window function has a smoothing effect on the spectrum.

The window function U(f) is plotted in fig. 10.

Fig. 11 shows how the individual values of the estimate $\hat{S}(f)$ are arrived at, illustrated by the determination of a single value of the function $\hat{S}(f_0)$.

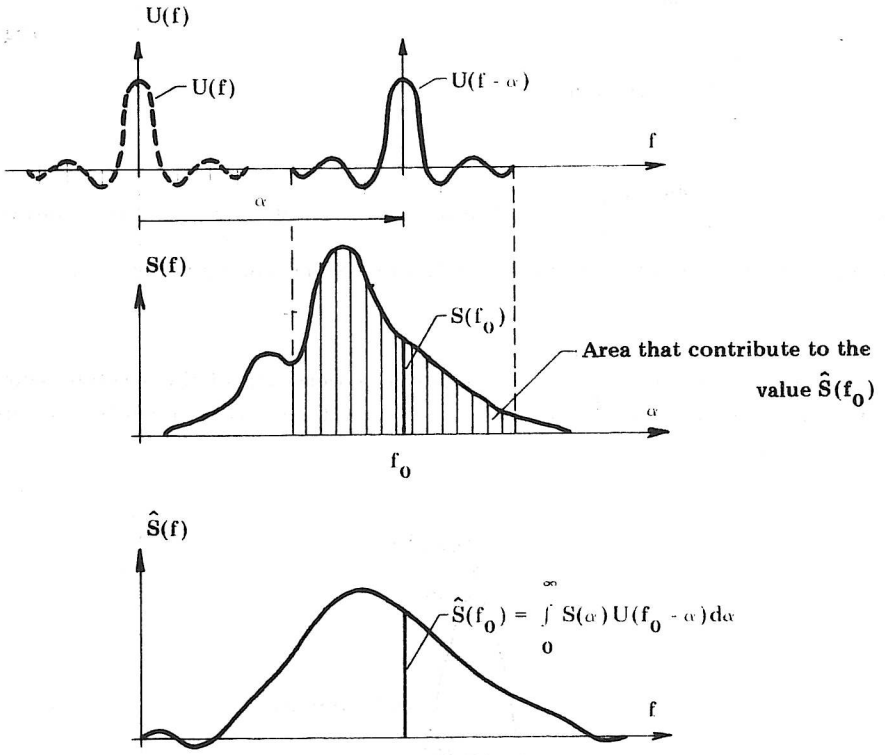

Fig. 11. Smoothing of the spectrum by means of a window function

It is apparent from the expression for the window function U(f) that the greater the value of τ_m (i.e. the better $R(\tau)$ is determined) the narrower the main lobe of U(f) will be, which again gives a greater resolution of the spectrum (less smoothing). The weakness of U(f) is the relatively large negative values of the second lobe, which in some cases can cause negative spectral values, socalled leakage. For this reason, window functions other than those given herein are usually used, but it

should be noted that any attempt to reduce the negative values results in a wider main lobe and a loss of resolution.

Since the negative values of the window function are due to the abrupt cut-offs of the boxcar function $u_{\tau_m}(\tau)$ at the ends ($\tau = \pm\tau_m$), one modifies $u_{\tau_m}(\tau)$ so that the values ramp out to zero at the ends, see fig. 12, that shows two very commonly used functions. Fig. 12a gives a window function of the type $U^2(f)$ whilst fig. 12b gives the »Hanning» window function,

$$D(f) = \frac{1}{4}U(f - \frac{1}{2}\tau_m) + \frac{1}{2}U(f) + \frac{1}{4}U(f + \frac{1}{2}\tau_m) \qquad (25)$$

which is shown (in frequency domain) in fig. 10.

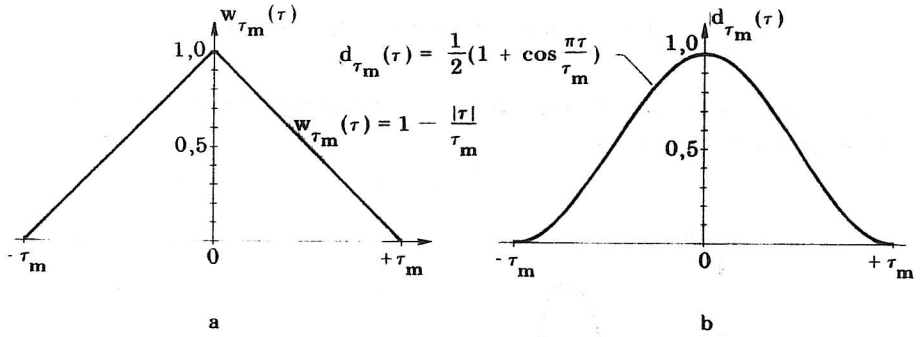

Fig. 12. Examples of window functions in time domain

The calculation of the energy spectrum described, by means of an autocorrellation function can be done purely electronically with an analoge voltage signal representing the wave surface $\eta(t)$, by speeding up the tape recorder. The calculation is most often done by computer, which is why we add some comments concerning problems which may arise in digital processing.

When selecting the rate of sampling the wave signal, it should be born in mind that low speeds can cause a distortion of the signal's frequencies. The phenomenon known as aliasing is shown in fig. 13, where the wave signal $\eta(t)$ for simplicity is shown as a periodic wave with frequency $f = 1/T$ and each sampling interval is called ΔT.

As seen in the figure, if the sampling interval $\Delta T > T/2 = 1/2f$ the signal frequencies are sensed smaller than actual. The effect is thus a cut-off of the frequencies above $f_c = 1/2\Delta T$, called the Nyquist or folding frequency. With respect to the energy spectrum the result is that the spectrum is cut-off at f_c and the energy

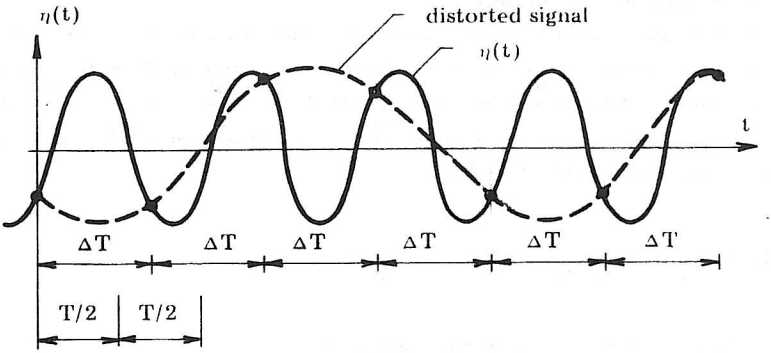

Fig. 13. Illustration of aliasing problem

of the frequencies above f_c is folded back into frequencies lower than f_c, i.e. a folding about f_c, see fig. 14.

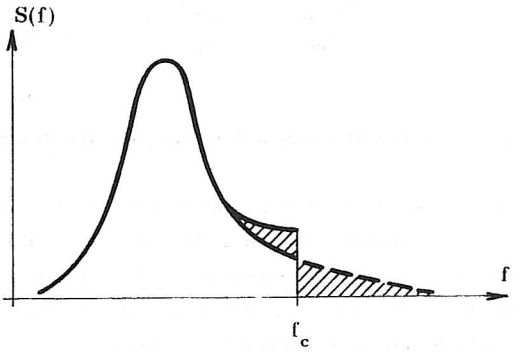

Fig. 14. Aliasing distortion of spectrum due to folding

To avoid this folding, the sampling interval must be $\Delta T \leq 1/2f_d$ where f_d is the highest frequency that is included in the wave signal. In practice one uses however a longer sampling interval when the wave energy of the frequencies above f_c is negligible. For example it is usual to use a sampling frequency of 2 sec^{-1} to analyse storm waves in the North Sea and other large seas. Another method is to filter the signal before sampling, so that the energy in the frequencies higher than those of interest is removed, whereupon f_c is selected equal to the cut-off fre-

quency. It should be noted that, although for economy one should set $\Delta T = 1/2f_d$, it is usually recommended to use $\Delta T \cong 1/3f_d$.

As already discussed, the limited length of the wave signal prevents us from determining the true energy spectrum; we have only an estimate $\hat{S}(f)$ of it. The question is then, how can we calculate the statistical inaccuracy of $\hat{S}(f)$ and what means do we have to limit the inaccuracy to an acceptable level.

A measure of the random portion of the estimation error is given by the normalized standard error, ϵ_r, defined as the standard deviation of the estimate divided by the true value

$$\epsilon_r = \frac{\sigma[\hat{S}(f)]}{S(f)} \tag{26}$$

It can be shown [3], that the normalized standard error of the estimate of the energy spectrum can be expressed as

$$\epsilon_r \cong 1/\sqrt{B_e T} \tag{27}$$

where T is the total duration of the wave signal and $B_e = 1/\int_{-\infty}^{\infty} U^2(f)\,df$ is the effective band width of the window function applied (see [14]), which in fact works as a filter. From fig. 10 we can see that $B_e \cong 1/\tau_m$, whereby

$$\epsilon_r \cong \sqrt{\tau_m/T} \tag{28}$$

Since it has further been shown [6] that as a close approximation $\hat{S}(f)$ is χ^2-distributed with $n \cong 2B_e T \cong 2T/\tau_m$ degrees of freedom (assuming $\tau_m \ll T$) this means that a $(1 - \alpha)$ confidence interval for S(f) based on the estimate $\hat{S}(f)$ will be given by

$$\frac{n\hat{S}(f)}{\chi^2_{n,\alpha/2}} \leqslant S(f) < \frac{n\hat{S}(f)}{\chi^2_{n,1-\alpha/2}} \qquad \text{where } n \cong 2T/\tau_m \tag{29}$$

(27), (28) and (29) show that a small random error or a large statistical confidence, require that $\tau_m \ll T$. Since for characterisation one can hardly use wave recordings shorter than the ca. 20 minutes (100-200 waves) commonly used, in practice, this means that we can only alter τ_m. In other words, one has to select a suitable small τ_m from (28) or (29).

Unfortunately, the circumstances are such that the smaller one selects τ_m, the poorer the resolution becomes, i.e. more details are lost in the spectrum, see fig. 10 and 11. Generally this means that the distance between the crests and the troughs in the spectrum is reduced. In addition the spectrum is defined with fewer points, since the autocorrelation function (22) and hence the spectrum have only $\tau_m/\Delta T$ points, where ΔT is the step interval of the digital wave signal. Taking for example the sampling interval $\Delta T = 1/2f_c$, where f_c is the Nyquist frequency, we get the spectrum in the range $0 \leq f \leq f_c$ defined with an interval Δf between points

$$\Delta f = \frac{f_c}{\tau_m/\Delta T} = \frac{1}{2\tau_m} \tag{30}$$

Δf is called the spectral band width, not to be confused with the previously mentioned effective band width $B_e \cong 1/\tau_m$, which refers to the weight function. Fig. 15 illustrates the effect of reducing τ_m.

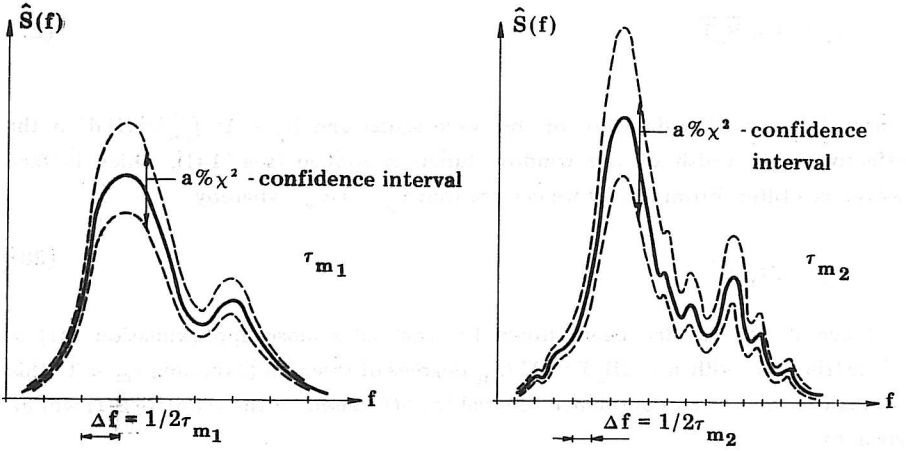

Fig. 15. Illustration of spectrum estimates corresponding to two values of τ_m. $\tau_{m1} < \tau_{m2}$.

The selection of τ_m has thus to be a compromise between the conflicting requirements. Normally a displacement τ_m of about 5 - 10% of T is used.

Apart from the purely statistical error, instrument errors (wave sampling and recording instruments) can of course occur, as well as errors due to non-stationarity of the wave signal.

3.2 Periodogram (FFT) method

Like the correlogram method, the FFT method is designed to calculate an estimate of the energy spectrum from a wave recording, but instead of working through the correlation function, the estimate is made directly by means of the socalled Fast Fourier Transform (FFT) algorithm. The idea behind the method, which is described throroughly in [14] among others, will be described briefly, whereas the uncertainties of the method will be discussed more thoroughly.

The method is based on the common Fourier expansion of a time series x(t), which in our case is the wave signal $\eta(t)$ of length T_p. Since the signal is assumed periodic with a period T_p and thereby has a basic frequency $f_1 = 1/T_p$ we get

$$x(t) = \frac{a_0}{2} + \sum_{q=1}^{\infty}{}' a_q \cos 2\pi q f_1 t + b_q \sin 2\pi q f_1 t$$

where

$$a_q = \frac{2}{T_p} \int_0^{T_p} x(t) \cos 2\pi q f_1 t \, dt$$

$$q = 0, 1, 2, \cdots \qquad (31)$$

$$b_q = \frac{2}{T_p} \int_0^{T_p} x(t) \sin 2\pi q f_1 t \, dt$$

For each frequency qf_1, we thus have a cosine amplitude a_q and a sinus amplitude b_q, which as discussed under wave spectrum, can be combined into a single amplitude, the half square of which is the variance of the frequency qf_1.

Since x(t) is digitalised into N number of discrete points with equal intervals $h = T_p/N$, and x(t) is therefore described by x(nh), where n = 0, 1, 2, · · · · ·, (N - 1), becomes the discrete form of (31)

$$a_q = \frac{2}{N} \sum_{h=0}^{N-1}{}' x(nh) \cos 2\pi q \frac{n}{N}$$

$$q = 0, 1, 2, \cdots \qquad (32)$$

$$b_q = \frac{2}{N} \sum_{n=0}^{N-1}{}' x(nh) \sin 2\pi q \frac{n}{N}$$

We now found that the determination of the Fourier constants from (32) will need about N real (non-complex) multiply-adds operations, which in practice will be of the order of $\geqslant 10^6$ operations.

The purpose of FFT is to reduce the number of operations by decomposing the series x(nh) into a number of shorter series and carry out Fourier transforms over each of these series. If we divide for example the series into two series with N_1 and N_2 discrete values respectively, the number of operations becomes approximately $N_1^2 + N_2^2 < (N_1 + N_2)^2 = N^2$. The method can be illustrated as follows:

The Fourier coefficients for an infinite series x(t) is given in complex form by

$$X(f) = \int_{-\infty}^{\infty} x(t)\exp(-i2\pi ft)\,dt \tag{33}$$

X(f) is called the Fourier transform of x(t).

Since our series is limited to the interval $0 \leqslant t \leqslant T_p$, we define the Fourier transform now as

$$X(f, T_p) = \int_{0}^{T_p} x(t)\exp(-i2\pi ft)\,dt \tag{34}$$

which in discrete form becomes

$$X(f, T_p) = h \sum_{n=0}^{N-1} x(nh)\exp(-i2\pi fnh) \tag{35}$$

where h, n and N are defined in connection with (32).

Let $X(f, T_p)$ be determined by frequency f_k, given by

$$f_k = \frac{k}{T_p} = \frac{k}{Nh} \qquad \text{where } k = 0, 1, 2, \text{----}, (N-1) \tag{36}$$

To simplify the notation we introduce $X_k = X(f_k, T_p)/n$ and $X_n = x(nh)$ whereby we get

$$X_k = \sum_{n=0}^{N-1} x_n \exp(-i2\pi kn/N) \tag{37}$$

Out of series x_n we now create two shorter ones y_n and z_n given by

$$y_n = x_{2n}, \quad z_n = x_{2n+1} \quad ; \quad n = 0, 1, 2, \text{------}, (N/2 - 1).$$

It can be seen that these two series together contain all the elements of x_n. The Fourier transform of x_n (37) is subdivided as follows,

$$\begin{aligned} X_k &= \sum_{n=0}^{N/2-1} x_{2n} \exp(-i 2\pi k 2n/N) + \sum_{n=0}^{N/2-1} x_{2n+1} \exp(-i 2\pi k(2n+1)/N \\ &= \sum_{n=0}^{N/2-1} y_n \exp(-i 2\pi k n/(N/2)) + \sum_{n=0}^{N/2-1} z_n \exp(-i 2\pi kn/(N/2)) \exp(-i 2\pi k/N) \\ &= Y_k + \exp(-i 2\pi k/N) Z_k \end{aligned} \tag{38}$$

where we have introduced the notations Y_k and Z_k for the Fourier transform of y_n and z_n respectively and the notation w for the factor of Z_k.

(38) shows that X_k will now only be defined in the frequencies corresponding to $0 \leqslant k \leqslant (N/2 - 1)$, whereas we want a frequency range of $0 \leqslant k \leqslant (N - 1)$.

However, the following can be proved [14]

$$Y_{k-N/2} = Y_k \qquad \text{and} \qquad Z_{k-N/2} = Z_k$$

whereby (38) can be rewritten to

$$X_{k+N/2} = Y_k - w Z_k \qquad \text{where } k = 0, 1, 2, \text{----}, N/2 - 1) \tag{39}$$

Y_k and Z_k can be split up in a similar manner by setting

$s_n = y_{2n}$, $r_n = y_{2n+1}$, $u_n = z_{2n}$, $v_n = z_{2n+1}$; $n = 0, 1, 2, \text{----}, (N/4 - 1)$

etc.

By selecting the number of data points $N = 2^P$ where P is a positive integer, the calculations can be taken to n = 0, 1, whereby X_k and thereby $X(f, T_p)$ can be easily found.

Let us assume that we have a 20 min. wave recording, sampled at 2 Hz, giving us about 2400 points. It we select p = 11, N is 2048, which is close enough to 2400. The Fourier constants X_k, and thus the energy spectrum, can now be found with the FFT process. The resulting estimate of the spectrum has shortcomings which are explained in the following.

In (33) and (34) we can see that $X(f, T_p)$ can be considered as the transform of an infinitely long signal y(t) multiplied by a boxcar function, which is defined only in the interval T_p. Changing the interval from $(0, T_p)$ to $(-T_p/2, T_p/2)$ for simplicity, we get

$$X(f, T_p) = \int_{-T_p/2}^{T_p/2} x(t)\exp(-i2\pi ft)dt = \int_{-\infty}^{\infty} u_{T_p/2}(t)y(t)\exp(-i2\pi ft)dt \qquad (40)$$

where y(t) assumes the same values in the interval $(-T_p/2, T_p/2)$ and where $u_{T_p/2}(t)$ assumes the value 1 in the interval $(-T_p/2, T_p/2)$ and zero elsewhere. This boxcar function is similar to that discussed in (23) except that the range is now T_p instead of $2\tau_m$. The Fourier transform of $u_{T_p/2}(t)$ is $U_{T_p/2}(f) = T_p\left(\frac{\sin\pi fT_p}{\pi fT_p}\right)$, that has the first zero crossing at $f = \pm 1/T_p$. This window function is otherwise quite similar to that of U(f) shown in fig. 10, and we can similarly have negative values in this approximation of the spectrum. This leakage is reduced by tapering the values of x(t) at each end of the range $(-T_p/2, T_p/2)$. Before we do the Fourier transform with FFT, we multiply therefore x(t) by a window function, the shape of which is illustrated in fig. 16, which shows a socalled cosine taper window function. The values are thus ramped out over length $T_p/10$ at each end.

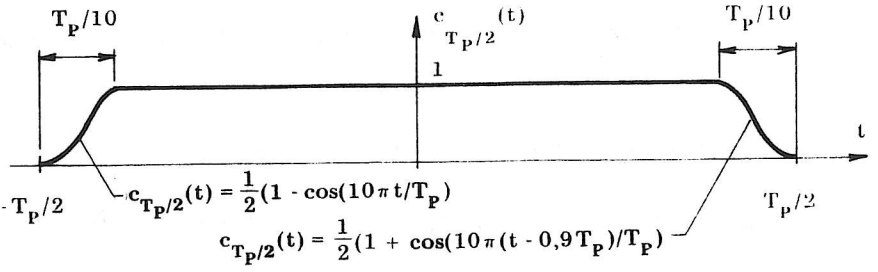

Fig. 16. Cosine taper data window

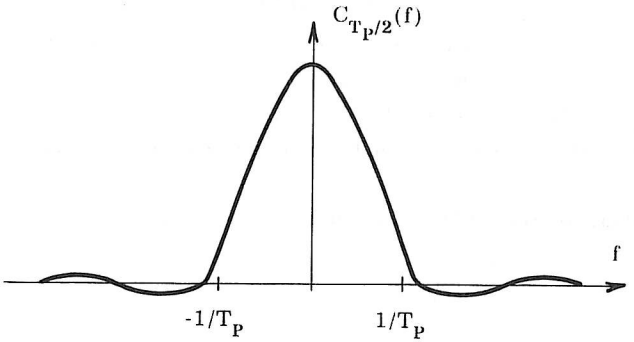

Fig. 17. Window function in frequency domain

Fig. 17 shows the Fourier transform of the cosine taper function and we can see that the leakage effect is strongly reduced at the expence of a slight increase in the main lobe width. From the figure it will be noted that the effective band width can be closely approximated to $B_e = 1/T_P$. The use of a cosine taper function instead of the carbox function results in spectrum estimates which are slightly too small since the area of the cosine taper function is slightly smaller than that of the boxcar function. The estimated spectrum values must thus be multiplied by a factor equal to the ratio of areas $A_{boxcar}/A_{costaper} = 1/0.875$.

An estimate of the energy (variance) of each of the frequencies given by (36) can now be found as

$$\hat{E}(f) = \frac{1}{2}|\, 2X_c(f, T_P)|^2 \, \frac{1}{0{,}875} \tag{41}$$

where the complex number $X_c(f, T_P)$ is the Fourier transform of $x(t)c_{T_P/2}(t)$.

The factor 2 is due to $X(f, T_P)$ referring to the two-sided variance spectrum, see fig. 9.

The estimate of the continuous energy spectrum, with frequency steps of $1/T_P$, is now

$$\hat{S}(f) = \frac{\hat{E}(f)}{1/T_P} = \frac{2}{T_P}\,|X_c(f, T_P)|^2 \, \frac{1}{0{,}875} \tag{42}$$

To end this chapter we shall now investigate the statistical uncertainty, i.e. the random error, of the estimate $\hat{S}(f)$.

$\hat{S}(f)$ is proportional to $|X_c(f, T_p)|^2 = (ReX_c)^2 + (ImX_c)^2$, where Re and Im refer to the real and imaginary parts respectively. Since the wave surface, described by $x(t)$, is assumed Gauss-distributed, and since the Fourier transform is a linear process ReX_c and ImX_c will also be Gauss-distributed quantities, about which it can be proved that they are uncorrelated random variables with equal variance and zero mean.

Every ordinate of $\hat{S}(f)$ will therefore have a distribution

$$\frac{\hat{S}(f)}{S(f)} = \frac{\chi_2^2}{\overline{\chi_2^2}} = \frac{\chi_2^2}{n} = \frac{\chi_2^2}{2} \tag{43}$$

where $n = 2$ is the degree of freedom. Note that an increase in the length of the wave signal T_p does not, in any way, alter the distribution and thereby the random error either. The only effect is that the spectrum values are determined over more frequencies.

We will now investigate the random part of the error in $\hat{S}(f)$ by calculating the normalised standard error, see (26),

$$\epsilon_r = \frac{\sigma[\hat{S}(f)]}{S(f)} = \frac{\sigma[\chi_2^2]}{\overline{\chi_2^2}} = \frac{\sqrt{2n}}{n} = 1 \tag{44}$$

since the mean value and standard deviation of χ_n^2 are n and $\sqrt{2n}$ respectively, and $n = 2$. In other words, the standard deviation of the estimate is of a magnitude similar to the quantity we are estimating. A random error of this magnitude is not acceptable, and we must thus use an averaging technique, either by ensample smoothing or frequency smoothing. As we usually only have a single sample (the wave recording) at our disposal, the latter solution is the only one possible.

Smoothing can, for example, be done by taking means over a row of continuous values of $\hat{S}(f)$. By averaging over 2 m values, (m = 1, 2, 3, - - - -) we get the following improved smoothed estimate of the raw estimate $\hat{S}(f)$

$$\tilde{S}(f) = \frac{1}{2m}\left[\hat{S}\left(f - \frac{m}{T_p}\right) + \text{- - - -} + \hat{S}(f) + \text{- - - -} + \hat{S}\left(f + \frac{m-1}{T_p}\right)\right] \tag{45}$$

Since each value of $\hat{S}(f)$ is a χ^2-variable with two degrees of freedom, we can conclude by means of the χ^2-addition theorem for independent variable that the improved estimate $\tilde{S}(f)$ will be χ^2-distributed with $n = 2 \times 2m = 4m$ degrees of free-

dom. The normalised standard deviation is then, se (44),

$$\epsilon_r = \frac{\sqrt{2n}}{n} = \frac{\sqrt{8m}}{4m} = \sqrt{\frac{1}{2m}} \tag{46}$$

which shows, that the random error can be reduced by increasing the number of points in the averaging.

The effect is illustrated in fig. 18 and we see that the effect of the averaging is similar to that of a trapeziodal spectral window built up of a number of window functions shown on fig. 17. An approximate value of the effective band width is $B_e' = 2m/T_P$, which with n = 4 m gives the relations

$$n = 2B_e' T_P \tag{47}$$

$$\epsilon_r = \frac{1}{\sqrt{B_e' T_P}} \tag{48}$$

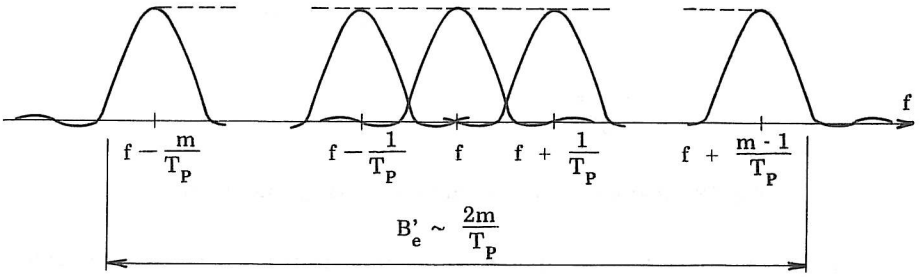

Fig. 18. Trapezoidal spectral window after frequency smoothing

A $(1 - \alpha)$ confidence interval for S(f) based on the smooth spectral estimate $\tilde{S}(f)$ will be given by

$$\frac{n\tilde{S}(f)}{\chi^2_{n,\alpha/2}} \leqslant S(f) \leqslant \frac{n\tilde{S}(f)}{\chi^2_{n,1-\alpha/2}} \tag{49}$$

where $n = 2B_e' T_P$.

It must be emphasized, that the random error cannot be indiscriminately reduced by increasing m (and thereby n), as averaging over many frequencies gives a poor resolution as well as a chance for bias errors. This is illustrated in fig. 19, that shows how the estimated $\tilde{S}(f)$ can deviate from $S(f_0)$ by averaging over a frequency interval B_e'.

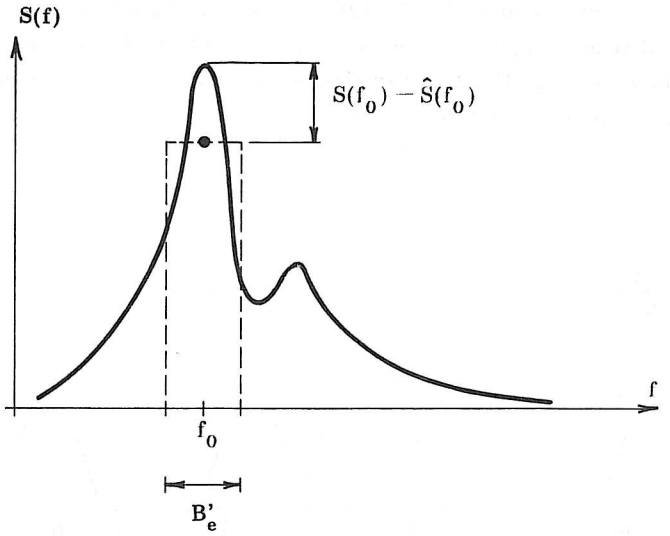

Fig. 19. Bias error introduced by frequency smoothing

In practice m must thus be chosen with due consideration to an acceptable statistical uncertainty and to a suitable resolution.

In the calculation of the wave spectrum of a 20 min. wave recording from a large sea, 2m = 16 or 32 will give reasonable results.

To end this chapter, it should be mentioned that the calculation of the spectrum by FFT has practically replaced the correlogram method because the FFT method is simpler (more direct), uses less computer processing time and retains more information. The latter is due to the fact that the calculation of the autocorrelation estimate inherently cause a smoothing of the spectra.

3.3 Standard wave energy spectra

In many locations, wave recordings are not available to give a basis for the calculation of the energy spectrum. In such cases, from a knowledge (or estimate) of the wind conditions alone it is possible to calculate characteristic values of wave height H and period T by empirical data plotted in wave prediction curves (fetch-diagrams). To determine the spectrum, some assumptions concerning it's shape and relation to the parameters H and T must be made. Since a consistent theoretical derivation of the energy spectrum is not yet available (only the higher frequency part of the energy spectrum function, which follows f^{-5}, seems to be theoretically well founded [7]), our knowledge relies essentially on empirical data. There are many suggestions for wind generated wave energy spectra, all based on agreement with wave recordings. We shall here discuss only two spectra, which, apart from being the most commonly used, are different in principle with respect to the wave condition they represent. Both spectra belong to the group of one-dimensional spectra, i.e. spectra with energy distributed over a frequency range only. This is of course a simplification of the true conditions, since wind energy is transferred to waves propagating in all directions within approx. 45° on either side of the wind direction. The latter is described by socalled directional spectra, which we shall however not discuss here.

In 1964, W. J. Pierson and L. Moskowitz put forward, on the basis of a similarity theory by S. A. Kitaigorodskii [8], some suggestions for deep water spectra for the sea state referred to as »fully arisen sea» [9]. This wave condition refers to the case where the waves have reached an equilibrium state in which energy input from the wind is exactly balanced by energy loss. The only variable is thus the wind velocity, which thereby determines the wave energy magnitude and distribution over the frequency range. It is important to emphasize, that spectra of this sort can only be hold valid, when the fetches are long enough for this equilibrium to be reached.

Out of the three analytical expressions suggested by Pierson and Moskowitz, the one below was found to give the best agreement with empirical wave data, and this spectrum is the one commonly known as the Pierson Moskowitz (or simply P. M.) spectrum

$$S(f) = \frac{\alpha g^2}{(2\pi)^4} f^{-5} \exp(-0.74(\frac{f_0}{f})^4) \qquad (50)$$

where $\alpha = 0.0081$

g = acceleration of gravity

$f_0 = g/2\pi U_{19.5}$, $U_{19.5}$ is the wind velocity at 19.5 m above still water level.

Instead of wind velocity, it is possible to insert a characteristic wave height and a characteristic wave period as parameters. If we insert the significant wave height H_s, and the average zero-crossing period T_z, that can be closely approximated by $H_s \cong 4\sqrt{m_0}$ and $T_z \cong m_0/m_1$ in terms of the spectrum moments, ref. [7] and [15], we can transform (50) to

$$S(f) = 0.11 \frac{H_s^2}{T_z^4} f^{-5} \exp(-0.44(T_z f)^{-4}) \tag{51}$$

An estimate of the peak-frequency, f_m (i.e. the frequency at which the spectral density is greatest) can be obtained from the relation $f_m \cong 0.65\, T_z^{-1}$.

Both (50) and (51) can be written in the following general form

$$S(f) = Af^{-5} \exp(-Bf^{-4}) \tag{52}$$

where A and B are independent of f. All spectra of this form are said to belong to the class of P. M. spectra.

Fig. 20 shows an example of a P. M. Spectrum for the 50 year storm in the north-east area of the Arabian Gulf. The spectrum is for a 13 m/sec south-west wind, in which direction there is a fetch of about 500 km.

The other wave spectrum which we shall deal with, is from The Joint North Sea Wave Project (usually shortened to JONSWAP), that was started in 1967 as a collaboration among institutes in West Germany, Holland, U.K. and USA [10]. The objective of the project was originally partly to investigate the growth of waves under conditions where the wave height is limited by the length of the fetch, and partly to investigate the change in the wave form as the waves move in from the sea into areas shallowing gradually. Simultaneous measurements of waves and wind were taken at stations along a line extending 160 km in a westerly direction from the island of Sylt in the German Bight.

A typical result of the recordings are given in fig. 21, which shows the spectra for a number of stations in wind conditions of steady easterly wind, approximately evenly distributed over the experimental area.

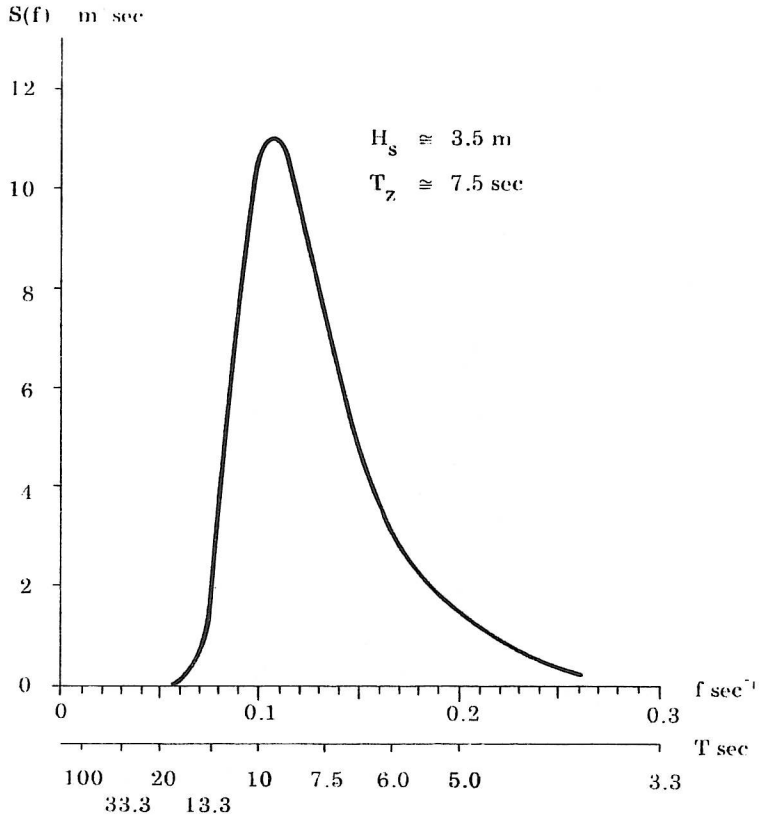

Fig. 20. Example of the Pierson - Moskowitz spectrum

Here it can be seen that both the maximum spectral density and the peak frequency are dependent on the length of the fetch. The figure also shows the socalled overshoot in which the energy at a particular frequency near the peak of the spectrum is nearly twice as large as the energy at the same frequency in a fully arisen sea, when an increase in the length of the fetch does not change the energy density about the frequency in question. Without going deeper into this phenomenon, it should be noted that from the study of the energy balance during the growth of the wave (the project's main objective) the overshoot phenomenon, as well as the shift of the peaks towards the lower frequencies, was explained by non-linear interactions between wave components, an effect which, incidentally,

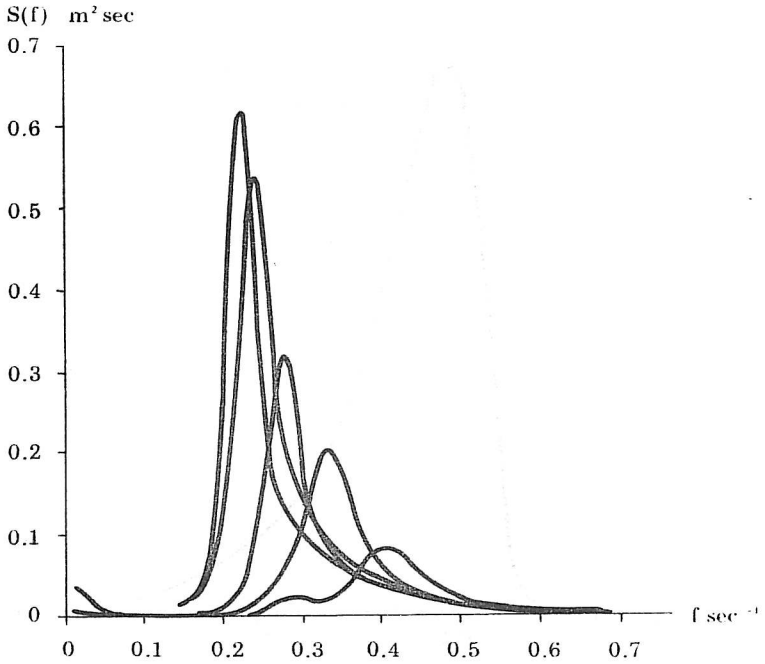

Fig. 21. Fetch limited spectra from JONSWAP project

is responsible for about 60% of the energy increase in the low frequency part of the spectrum.

During the processing of a large number of spectra, all generated under the same ideal wind condition referred to in the earlier comment to fig. 21, the following expression, which gives the so-called JONSWAP (or simply J) spectrum, was derived

$$S(f) = \frac{\alpha g^2}{(2\pi)^4} f^{-5} \exp\left(-\frac{5}{4}\left(\frac{f_m}{f}\right)^4\right) \gamma^{\exp\left(-\frac{1}{2}\left(\frac{f-f_m}{\sigma f_m}\right)^2\right)} \tag{53}$$

where

$\alpha = 0.076 x^{-0.22}$

$x = g F U_{10}^{-1}$ F is the length of the fetch, U_{10} is the wind velocity at a height of 10 m above still water level

$$f_m = 3.5 g x^{-0.33} \quad \text{peak frequency}$$

$$\gamma = 3.3 \quad \text{(mean value)}$$

$$\sigma = \begin{cases} 0.07 \text{ for } f \leq f_m \\ 0.09 \text{ for } f > f_m \end{cases}$$

By comparison with (50) it is apparent that the Jonswap spectrum, in principle, is made up of the P.M. spectrum multiplied by the factor

$$\gamma^{\exp(-\frac{1}{2}(\frac{f-f_m}{\sigma f_m})^2)}$$

It is also possible to insert the parameters H_s and T in the Jonswap spectrum, for example as suggested in [11] and [12].

After publication of the Jonswap spectrum, a large number of wave spectra for waves generated in limited fetch under non-stationary and inhomogeneous wind conditions have been analysed, whereby it has been proved, that these spectra are also of the Jonswap type. With this background, the Jonswap spectrum is generally applied to wave conditions of limited fetch (growing waves). It should, however, be noted that one does not have much knowledge to date of the transition from the limited fetch to the fully developed balanced conditions, for which the P. M. spectrum is valid. The Jonswap project — with a maximum fetch of 160 km — could not clarify these circumstances.

It should further be noted, that experience shows, that the Jonswap spectrum gives a better agreement with the recorded storm wave conditions in the North Sea, than the P. M. Spectrum. The Jonswap spectrum is sharper and has a larger concentration of energy about the peak frequency than the P. M. spectrum. One should, incidentally, be wary of comparing the two spectra directly since they refer to different wave conditions.

4. DETERMINATION OF THE HYDRODYNAMIC TRANSFER FUNCTION

In this chapter we shall see how, purely practically, estimates of the transfer function can be determined.

In section 2.4 we found the following expression for the transfer function valid for discrete frequencies,

$$|H(f_i)|^2 = \frac{\frac{1}{2}a_\lambda^{\,2}(f_i)}{\frac{1}{2}a_\eta^{\,2}(f_i)} = \left(\frac{a_\lambda(f_i)}{a_\eta(f_i)}\right)^2 \tag{54}$$

i.e., the value of the transfer function is obtained from the square of the ratio of the amplitudes of the force and the wave.

Corresponding values of the two amplitudes can be found

a. either by a deterministic calculation of the wave force amplitude a_λ, corresponding to a regular wave $a_\eta \cos(\omega t)$ for a number of frequencies,

b. or by model tests to measure the force amplitude and wave amplitude for regular waves with a number of frequencies. The wave measurement must be taken at a point where the wave conditions represent the wave condition undisturbed by the structure, or else by measuring the waves at the location before the structure is set in place.

In section 2.4 we also found the following connection between the transfer function and the spectra of the wave force and wave amplitude

$$|H(f)|^2 = \frac{S_\lambda(f)}{S_\eta(f)} \tag{55}$$

We note here from, that the transfer function can also be determined

c. by generating irregular waves (not periodic) in a model test and take measurements (preferably simultaneously) of the wave amplitude and force amplitude signals, from which $S_\lambda(f)$ and $S_\eta(f)$ can be determined, for example by FFT, see section 3.2. As in alternative b, it is important that the wave amplitude signal represents the wave conditions undisturbed by the structure.

Finally a useful relationship is stated by means of which the gain factor (the absolute value of the frequency response function H(f)), which is the square root of the transfer function, can be determined (for further explanation see [3]).

$$|H(f)| = \frac{|S_{\eta\lambda}(f)|}{S_\eta(f)} \tag{56}$$

$S_{\eta\lambda}(f)$ is the cross-spectral density function defined as the Fourier transform of the cross-correlation function $R_{\eta\lambda}(\tau)$ i.e.

$$S_{\eta\lambda}(f) = \int_{-\infty}^{\infty} R_{\eta\lambda}(\tau)\, e^{-i2\pi f\tau}\, d\tau \tag{57}$$

where

$$R_{\eta\lambda}(\tau) = \lim_{T\to\infty} \frac{1}{T} \int_{0}^{T} \eta(t)\lambda(t+\tau)\, dt$$

From this it follows that the transfer function can furthermore be determined

d. in model tests, as described in alternative c, by measuring wave amplitude and force amplitude signals, from which $S_{\eta\lambda}(f)$ and $S_{\eta}(f)$ can be determined by correlogram or periodogram methods. Note that the cross-spectral density function contains information on the phase shift through the system.

Methods c and d enables us to find the confidence limits and thereby to get an idea of the random error of the transfer function. According to [3] the $1 - \alpha$ confidence interval for H(f) is given by

$$|\hat{H}(f)| - \hat{r}(f) \leq |H(f)| \leq |\hat{H}(f)| + \hat{r}(f) \tag{58}$$

where $\hat{r}^2(f) = \frac{2}{n-2} F_{2,n-2;\alpha} [1 - \hat{\gamma}_{\eta\lambda}{}^2(f)] \frac{\hat{S}_{\lambda}(f)}{\hat{S}_{\eta}(f)}$

n = degrees of freedom of each of the spectral estimates

$F_{2,n-2;\alpha}$ = 100α percentage point of an F distribution with $n_1 = 2$ and $n_2 = n - 2$ degrees of freedom

$\hat{S}_{\lambda}(f)$ = wave force spectrum estimate

$\hat{S}_{\eta}(f)$ = Wave energy spectrum estimate

$\hat{\gamma}_{\eta\lambda}{}^2(f)$ = sample estimate of the cohorence function

$$\gamma_{\eta\lambda}{}^2(f) = \frac{|S_{\eta\lambda}(f)|^2}{S_{\eta}(f) S_{\lambda}(f)}$$

The confidence interval of the transfer function is found by squaring the limits in (58). It is obvious that the random error is very dependent on the degrees of freedom of the spectral estimates. For small values of n, $\hat{r}^2(f)$ is very large and has a correspondingly large confidence interval. As seen in sections 3.1 and 3.2 the degrees of freedom will, however, hardly ever be less than 20 in practice. One should note that the bias error of the transfer function usually is of less consequence than the random error.

As an example of the methods a, b, c, and d we shall show the gain factor for the over all horizontal wave force (in the wave travel direction) on a model gravity platform, see fig. 22, that shows the platform's natural dimensions.

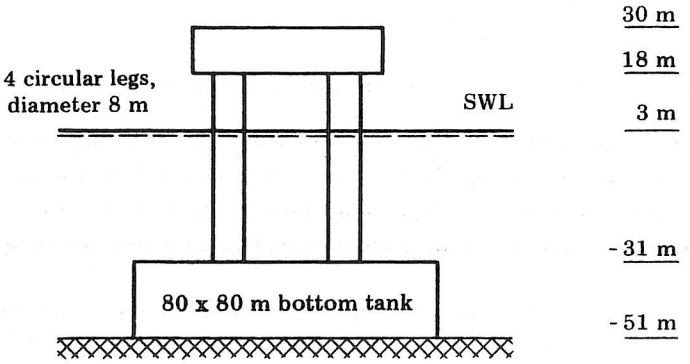

Fig. 22. Prototype gravity platform

The calculations and model tests were carried out at the Hydraulics and Coastal Engineering Laboratories, Aalborg University Center.

The model's linear scale was 1: 267. Two-dimensional (long crested) waves were used.

Fig. 23 shows a comparison of the gain factors determined by each of the four methods described. As can be seen there is a good correlation between the gain factor values estimated according to the methods b, c, and d. The measured values are also in good agreement with a calculated curve (method a), which has been found by calculating the horizontal component of the Froude - Krylov force on the bottom tank and multiplying it with a factor (see [15]), where upon the inertia forces from the 4 legs (calculated by means of the Morison's formula) have been added.

To end this section we shall show some results from an investigation of transfer functions for a surface piercing vertical cylinder, influenced by three-dimensional

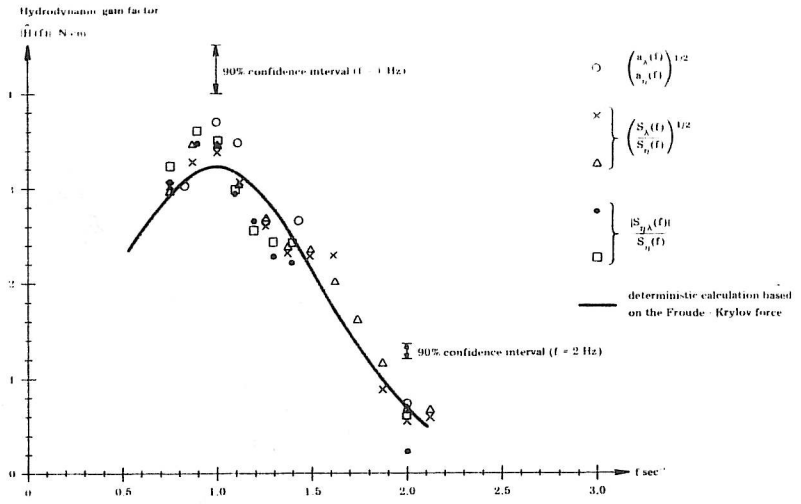

Fig. 23. Estimates of the hydrodynamic gain factor for over all horizontal wave forces (in wave travel direction) on a model gravity platform

(short crested) waves, [13]. The investigation was carried out by the Hydraulics Research Station, Wallingford in England, who have a wave tank fitted with 10 independent wave generators, which together can create a wave field with a given energy spectrum and a given angular spread of wave energy. Wave conditions that resemble very closely those existing in nature can thus be created.

The cylinder tested, with a diameter of 60 cm, was exposed to waves partly with a P. M. spectrum of $H_s \cong 15$ cm and a mean zero crossing periode $T_z \cong 1.5$ sec., and partly with a sharper spectrum (resembling the Jonswap spectrum) of $H_s \cong 11.5$ cm and $T_z \cong 1.1$ sec. The diameter of the cylinder in these circumstances was so large, relative to the wave lengths in the essential part of the spectra, that the cylinder modified the wave field. The circumstances were thus those of the diffraction-inertia regime, where the drag forces can be neglected and where a calculation of wave forces must be done with due regard to the diffracted waves.

Fig. 24 shows the hydrodynamic gain factor |H(f)| (square root of the transfer function) for the horizontal wave forces, partly in the main direction of transplantation of the wave energy (in-line) and partly at right angles (transversal). It is worthy of note that the lateral forces, which neither theoretically nor experimentally can be determined from two-dimensional waves, are about half as large as the in-line forces.

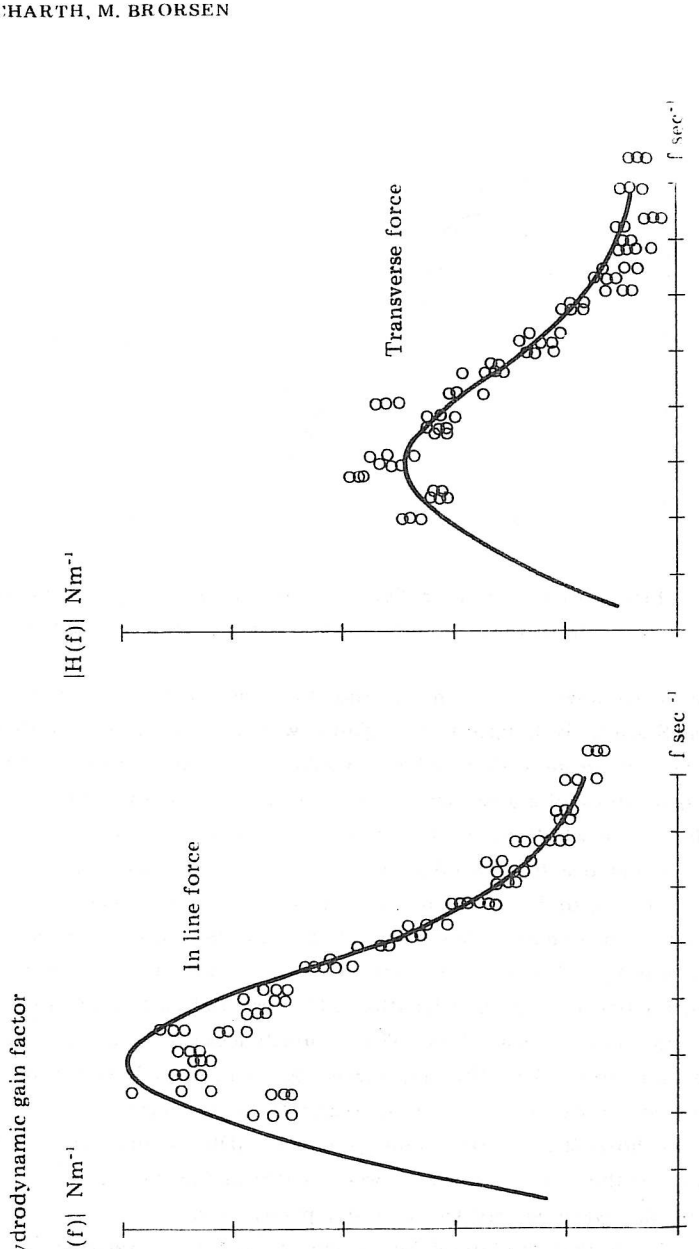

Fig. 24. Hydrodynamic gain factor for the over-all horizontal force on a cylinder in three-dimensional (short crested) irregular waves, with $\cos^2 \phi$ horizontal energy distribution.

The figure incidentally shows an amazingly good agreement between the test results and the theoretical calculations. The experimentally determined plots are found by dividing the measured wave load spectrum by the measured wave energy spectrum, that is to say by method c. Since the proper wave conditions could only be generated within a limited area, where the presence of the cylinder altered materially the waves in comparison to the undisturbed waves, it was impossible to find both spectra by simultaneous measurements. However, the »stochastic» signal that controls the wave generators can be repeated, enabling the waves to be measured before the structure was placed, without thereby increasing the statistic uncertainty.

The theoretical calculation of H(f) was done by means of the theory of diffraction for three-dimensional waves developed in connection with the investigation [13].

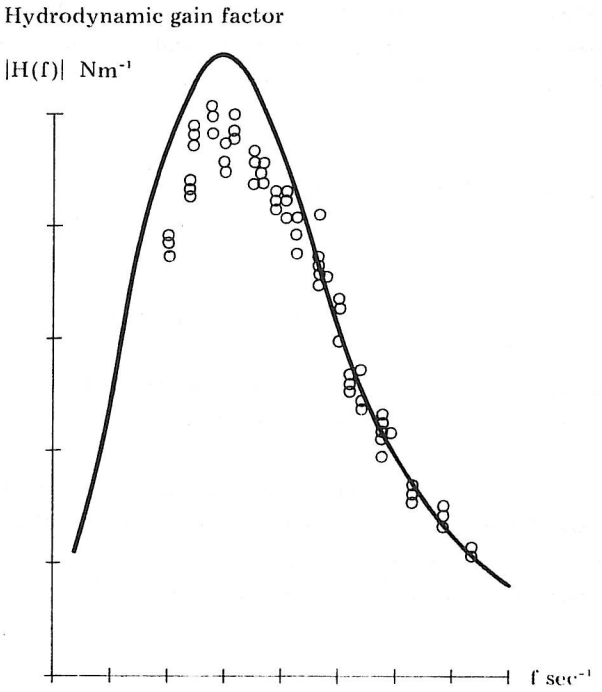

Fig. 25. Hydrodynamic gain factor for the over-all horizontal force on a cylinder in two-dimensional (long crested) irregular waves.

For a comparison, the results of corresponding tests with two-dimensional (long crested) waves are shown in fig. 25. It is apparent that the in-line forces differ relatively little from each other in the two tests.

5. DETERMINATION OF THE RESPONS SPECTRUM

In the previous section we saw how the wave load spectrum $S_w(f)$ corresponding to any given wave energy spectrum S(f) can be found by multiplying the energy spectrum by the hydrodynamic transfer function $|H(f)|^2$.

The wave load is, however, not the final loading on the structure unless this is infinitely rigid. In practice there will be a dynamic amplification of the wave load, that can be described by a so called mechanical transfer function M(f), which gives the relation between the wave load spectrum $S_w(f)$ and the final load spectrum, called the response spectrum $S_r(f)$. The relation between these spectra is given by

$$S_r(f) = |M(f)|^2 S(f) = |M(f)|^2 |H(f)|^2 S_w(f) \tag{59}$$

The conversion from wave energy spectrum to response spectrum can be illustrated as shown on fig. 26.

As a simple example of a calculation of the response spectrum, we shall consider the simplest possible approximation to a kinetic system, which represents a gravity platform.

We thus assume that the bottom of the sea and the base tank are infinitely rigid, that the tower (or towers) is fixed (encastré) in the base tank, that the displacement under wave action occurs in a plane, and that the combined mass of the system is concentrated as an equivalent mass at one point, see fig. 27.

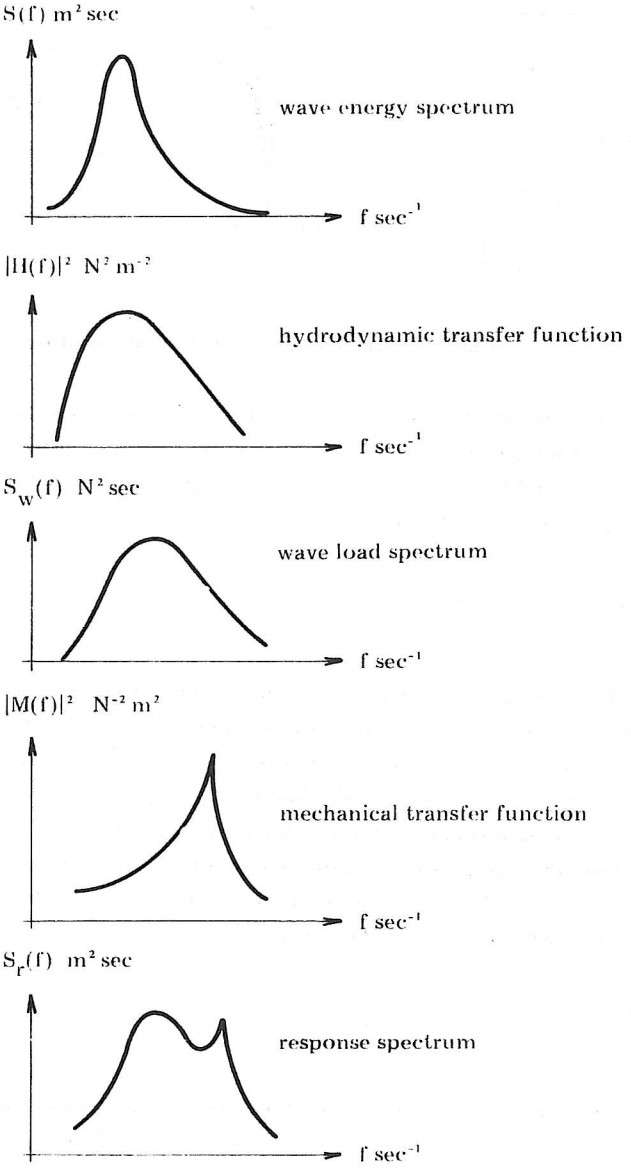

Fig. 26. **Steps in stochastic response analysis.**

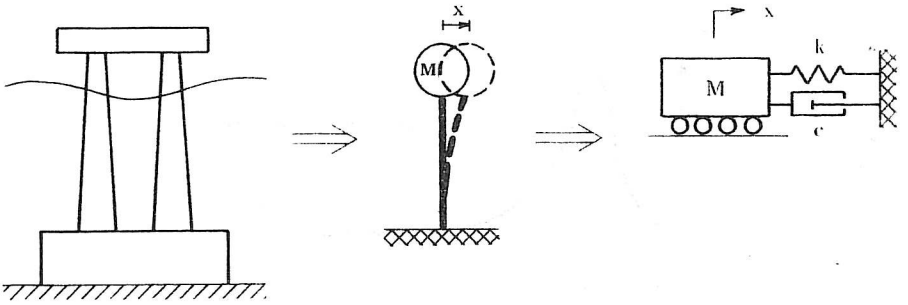

Fig. 27. One degree of freedom idealization

Since we only need a single co-ordinate x to specify the displacement of the system, the system has only one degree of freedom. x is the instantaneous position of the mass relative to the point of fixture. The equilibrium equation for the system is according to Newton's law of motion

$$M\ddot{x} + c\dot{x} + kx = F(t) \tag{60}$$

where M is the equivalent mass of the platform, towers and associated water (hydrodynamic mass), c is the sum of the hydraulic damping and the structural damping, k is the stiffness of the towers and F(t) is the wave load. It must be emphasized that in more realistic models than that of fig. 27 the sea bed will also contribute to both damping and stiffness in the terms c and k.

The frequency response function, which is here called the mechanical frequency response function M(f), is found by substituting F(t) with a periodic function $e^{-i2\pi ft}$ and x with $M(f)e^{-i2\pi ft}$. We thus get

$$M(f) = \frac{1}{k + i2\pi fc - m(2\pi f)^2} \tag{61}$$

whereby the mechanical transfer function $|M(f)|^2$ can be calculated.

Inserting $\omega = 2\pi f$, the natural frequency $\omega_n = \sqrt{k/m}$ and the damping ratio $\zeta = c/\sqrt{4\,km}$ we get the well-known expression

$$M(\omega) = \frac{1}{m(\omega_n^2 + i2\zeta\omega_n\omega - \omega^2)} \tag{62}$$

We note from (62) that resonance sets in when $\omega \cong \omega_n$ and the damping is small.

Concerning systems with more degrees of freedom, refer to [4].

6. DETERMINATION OF THE MAXIMUM LOADS

As mentioned in section 2.4, a Gaussian process which is transformed by a linear system remains Gaussian. The crests of both the wave force signal and that of the final response signal will therefore have the same distribution as the wave heights in the wave amplitude signal, in other words, a Rayleigh distribution.

The most probable maximum value grows with the length of the signal (number of waves). If we have a recording with N, number of waves, the probability for the largest wave H_{max} is given by

$$1 - F\{ H_{max} \} = \frac{1}{N} \tag{63}$$

where $F\{ H_{max} \}$ is the probability that the wave is smaller than H_{max}. The distribution function $F\{H\}$ for Rayleigh distributed wave heights is given by

$$F\{H\} = 1 - e^{-\frac{H^2}{8m_0}} \tag{64}$$

Inserting (64) in (63) and solving for H_{max}, we get the expected maximum value

$$H_{max} = 2\sqrt{2m_0}\,\sqrt{\ln N} = H_s\sqrt{\frac{\ln N}{2}} \tag{65}$$

where m_0 is the area under the wave energy (variance) spectrum and where we have utilized (15).

Since x denotes the amplitude of the structure's displacement, see fig. 27, we thus find that the expected maximum value of the amplitude in the course of N waves is

$$|x_{max}| = \sqrt{m_0}\,\sqrt{2\ln N} \tag{66}$$

where m_0 is now the area under the response spectrum.

It can be proved, ref. [2], that the probability that the maximum values obtained by (65) and (66) are exceeded in the course of N, number of waves, is about 63%.

The above extreme statistics refer to a given wave recording, whereby m_0 (and thereby H_s) are considered constant. We call this statistics, short-term statistics, and the corresponding distribution function, the short-term distribution. The moment m_0 however, varies from one wave recording to another, which is the reason why we must consider the distribution of m_0 in order to determine the long-term distribution which is used to determine the maximum loads expected to occur over some period of time. For further explanation se ref. [16].

7. REFERENCES

[1] D.E. Cartwright and M.S. Longuet-Higgins. The Statistical Distributions of the Maxima of a Random Function. Proc. Roy. Soc., Vol. 237, April 1956.

[2] Bølger på dypt og grunt vand, NTH 1976. Instituttet for Havnebygning. Norges Tekniske Højskole. Trondheim.

[3] J.S. Bendat and A.G. Piersol. Random Data. Wiley - Interscience. New York 1971.

[4] S.H. Crandall and W.D. Mark. Random Vibration in Mechanical Systems. Academic Press. New York 1973.

[5] J.H. Laning and R.H. Battin. Random Processes in Automatic Control. Mc Graw-Hill. New York 1956.

[6] R.B. Blackman and J.W. Tukey. Measurement of Power Spectra. Dover Publications. New York 1958.

[7] O.M. Phillips. The equilibrium range in the spectrum of wind generated ocean waves. Journal of Fluid Mechanics. Vol. 4. 1958.

[8] S.A. Kitaigorodskii. Applications of the theory of similarity to the analysis of wind generated wave motion as a stochastic process. Izv. Akad. Nauk. S.S.S.R. Ser. Geofiz Vol. 1. 1962.

[9] W.J. Pierson and L. Moskowitz. A proposed spectral form for fully developed wind seas based on the similarity theory of S.A. Kitaigorodskii. Journal of Geophysical Research, Vol.69, no 24, December 1964.

[10] K. Hasselmann et al. Measurements of wind-wave growth and swell decay during the Joint North Sea Wave Project. Deutsches Hydrographisches Zeitschrift. Hamburg Reihe A. Nr. 12. 1973.

[11] ISSC, Report Committee 1, 6th International Ship Structures Congress. Boston. 1976.

[12] O.G. Humb and T. Overvik. Parameterization of wave spectra and long term joint distribution of wave height and period. Proceedings Boss' 76, Vol. I, 1976.

[13] S.M. Huntington and D.M. Thompson. Forces on a large vertical cylinder in multi-derectional random waves. Offshore Technology Conference, Houston, Texas, 1976, paper no 2539.

[14] D.E. Newland. Random Vibrations and Spectral Analysis. Longman, London 1975.

[15] N. Hogben and R.G. Standing. Experience in Computing Wave Loads on Large Bodies. Offshore Technology Conference, Houston, Texas, 1975, paper no 2189.

[16] Environmental conditions of the Norwegian continental shelf. Oljedirektoratet, Stavanger, Norway.